Chapter 4

Inter-Operable Multi-Utility Fast Charger with V2Aux and V2V Capability

4.1 Introduction

Building upon the principles of fractional power processing (FPP) established in the previous chapter, this chapter introduces a novel application of FPP approach specifically tailored to address the multiple and complex power conversion demands of Electric Vehicle (EV) onboard. It is known that setting up a dedicated off-board charging facility require high capital cost and off-board space. Whereas, the on-board chargers have the flexibility to charge at one's convenience. However, due to their compact space the on-board chargers have limited and slow charging capability elongating the battery charging time [94]. Further, with the growing charging network across country and the reduced cost/km, consumers are considering them for long range and intercity travel. However, one of the challenge in taking longer routes is the diversity in nature of charging facility from city to highway.

The charging networks in cities are more focused on providing fast charging facilities suitable for short daily commute catering to lower voltage battery pack enabled EVs. Whereas, the highway networks are more focused towards the high-voltage high power charging generally comprising of Level 3 DC charging and ultra-fast charging facilities. This diversity in the charging network leaves a gap in interfacing the city and highway off-board facility and a direct connection might lead to the adverse effects on the EV battery life. Often times, the battery charging power gets limited to the power level of the on-board charger due to the rating mis-match [132]. Voltage matching between dc fast charger output and battery is achieved by operating the on-board dc/dc charger as an interface. However, the onboard charger with its limited rating cannot handle the entire power. To efficiently improve the flexibility of charging between AC, DC and high-power fast charging, an on-board charging interface that can handle significantly higher power is necessary [133].

To extend the power handling capability of the on-board charger to fast charging level existing literature suggest many approaches however, the cost of the components with increasing voltage level becomes impractical to be used for power level exceeding level 2 OBC, and thereby limiting their minimum charging time. With the continuous penetration of higher battery pack voltage, long-range EVs, and concerns on charging time, the trends on co-dependency of on-board charging and DC fast charging have been on a rise. It basically indicates an on-board charger design that performs slow AC charging as well as can facilitate DC fast charging, by bypassing the front-end AC/DC stage. Although this approach extends the charger adaptability to both AC and DC charging, but the charging capability remains limited to on-boards rated DC/DC converter.

In addition to the high voltage power train, the on-board power electronic involves low-voltage auxiliary loads that include power steering, automatic windows, controllers, fans, wipers, and additional luxury features, such as power sunroofs, active suspension systems, and entertainment systems, which can increase the required power rating of the auxiliary power module APM to significant load. Thus, the converter needs to regulate the output to supply constant voltage loads at high efficiency. Conventionally, an auxiliary power module comprising of a separate DC/DC converter was employed to supply auxiliaries. Recent literature reports integrating the APM to power train by re-utilizing the charger components to deliver auxiliaries, however the existing approaches suffered due to degraded efficiency at the low power. Further, vehicle-to-vehicle (V2V) charging is an economic and flexible approach to replenish EV battery on-the-move and alleviate range anxiety [134]. The existing approaches to enable V2V charging were performed through multiple operating stages that resulted in degraded efficiency whereas, the integrated charger approach required additional relays increasing the complexity and cost of the converter.

To address the above issue of the conventional on-board chargers, this chapter presents a novel interoperable multi-utility fast charger. A representative block diagram of the proposed charger incorporating all functions as a part of OBC is shown in Fig. 4.1. The charger addresses the problem of low charging power (slow charging speed) of the existing class of OBCs due to its capability to handle significantly higher power as is required in dc fast charging, without over-exploiting the existing ac-rated OBC components and performing high-efficiency fast charger while ensuring soft-switching

for entire operating range. It further eliminates the complex controller required in the existing state-of-the-art multi-utility converters to achieve different operating modes, and make use of the existing component capacity to facilitate V2Aux mode and V2V mode charging mode, ensuring efficient converter operation.

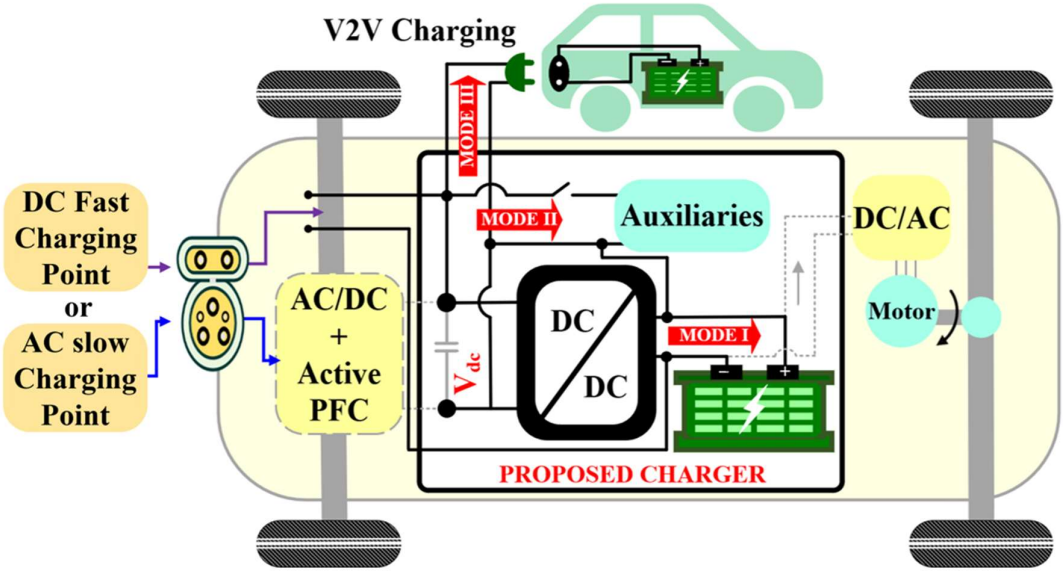

Fig. 4.1 Proposed interoperable multi-utility fast charger.

The chapter also examines recent research trends and technological innovations that have contributed to the development of high-performance interoperable multi-utility converters FPPs for EV charging applications.

4.2 Proposed Interoperable Multi-utility Charger

4.2.1 Circuit Configuration of the Proposed Multi-Utility Charger

The proposed charger is derived from a resonant dual active bridge converter to form a fractional power processing architecture that allows only a part of power to be processed through the converter, while allowing the major power to be transferred efficiently through direct series path. The proposed interoperable multi-utility charger can work as

- *AC Slow Charger* by interfacing ac/dc front-end stage operating as a full power processor in forward power flow mode.
- *DC Fast Charger* by operating as fractional power processor in forward power flow mode and resonant frequency.

- *V2Aux constant voltage regulating converter* operating as a full power processor in reverse power flow mode at half resonant frequency
- *V2V constant current charger* by operating as full power processor in reverse power flow mode at resonant frequency.

The circuit of the proposed charger is shown in Fig. 4.2. The dotted lines are colour coded to represent the connection in respective mode of operation. When operating in dc fast charging mode, the source V_{dc} appears in series with input of converter with $+V_{dc}$ connected to input capacitor C_{in} and negative terminal of V_{dc} connected to the negative terminal of battery, $-V_{bat}$. Further, C_{in} is connected to primary H-bridge composed of MOSFETs which is further connected to another MOSFET-based H-bridge through a high frequency transformer. Furthermore, the leakage inductance of the high-frequency transformer forms a parallel resonant tank circuit with the capacitor C_r connected at the output of the secondary bridge. Also, an inductor L_r in series with the battery is connected across C_r. The series by-pass path is further established by connecting $-V_{bat}$ to converter input negative $-V_{in}$. It may be noted that as soon as the source V_{dc} is plugged out, the series-bypass path of FPP configuration faces an open circuit, ultimately resulting in full-power processing configuration of the charger.

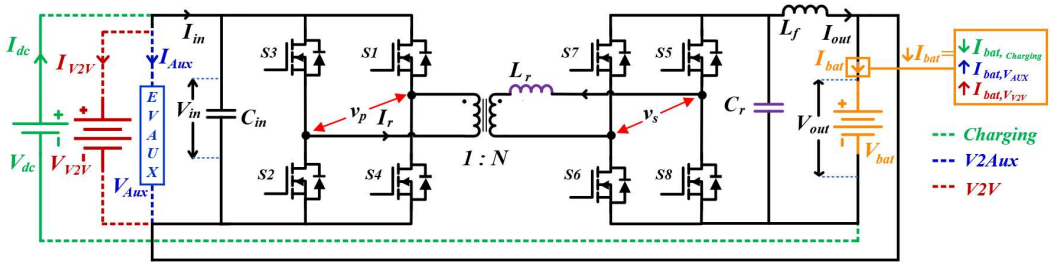

Fig. 4.2 Proposed inter-operable multi-utility fast charger with V2Aux and V2V capability

Further, the selection of MOSFETs for high-frequency switching bridges facilitates bi-directional operation of the proposed converter allowing fast charging of battery and battery to auxiliary as well as battery to vehicle charging modes of operation. In V2Aux mode and V2V mode, the circuit configuration remains the same and the mode implementation is achieved through appropriate switching strategy. A selection switch is used that connects auxiliary as a load during cruising or V2Aux mode. Further, when another vehicle's charging port has to be plugged in, the same switch disconnects the auxiliary loads. The parallel resonant tank circuit formed by L_r and C_r imparts the

constant current (CC) behavior implemented in fast charging and V2V charging mode, and constant voltage (CV) behavior implemented in V2Aux mode, respectively.

4.2.2 Working of the Proposed Charger in Each Mode

The OBC performs slow charging when connected to level 1 or level 2 charging outlet and the dc/dc converter operates on the output of front-end PFC ac/dc stage, at its OBC rated value. DC charging occurs when the EV charger is plugged into fast charging dc port. At this point, the V_{dc} is plugged-in and the series by-pass path is active, as shown in Fig. 4.3. Here, only a part of fast charging power, depending on the voltage V_{dc} is processed through converter and the major power flows through the series path which ideally is a lossless path, and practically incurs only conduction losses due to path resistance. This results in losses to only occur in the converter path. The direction of power flow and amount of current fed to the battery depends on the phase shift between the primary and secondary bridge. During this time the auxiliaries are inactive, as is also recommended for user safety. Further, as soon as the charging is complete the charger is plugged out from dc outlet, this breaks the outer circuit loop and conduction stops from bypass path, resulting in entire power to flow through the converter.

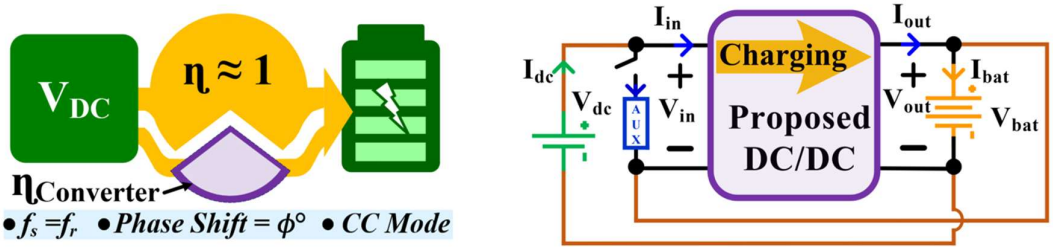

Fig. 4.3 Block diagram and equivalent circuit representation of proposed inter-operable multi-utility fast charger in FPP charging mode.

Now, when the charging is inactive, the propulsion battery acts as a source, and the auxiliary to be powered up is connected through a switch, as shown in Fig. 4.4. The converter works in reverse power flow mode, by operating primary bridge at lagging phase-shift with respect to secondary bridge. In addition, the switching is done at half-resonant frequency to drive the converter as a constant voltage source as required by the constant voltage auxiliary loads.

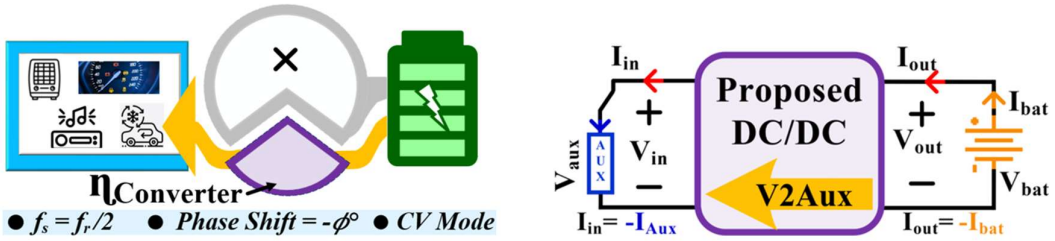

Fig. 4.4 Block diagram and equivalent circuit representation of proposed inter-operable multi-utility fast charger in Vehicle to auxiliary mode.

Now, in case when the EV acts as an emergency backup to another EV, the switch deactivates the auxiliary and another EV battery is plugged at the converter input port V_{in}, as shown in Fig. 4.5. Further, to charge another EV battery as a backup, a quick, 20-40% of SOC need to be added to the discharged battery, thus, the battery needs to be charged in constant current by operating the converter in full power processing mode, resonant frequency and at lagging phase shift.

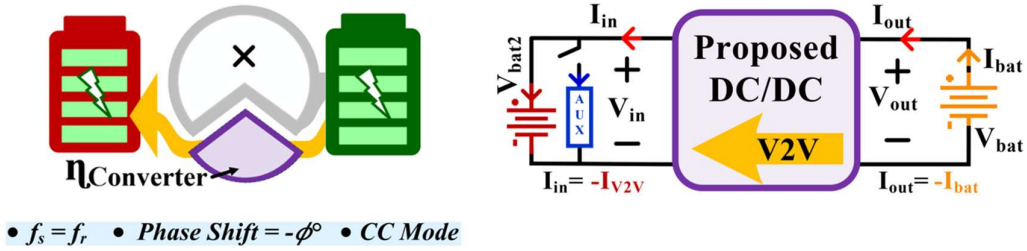

Fig. 4.5 Block diagram and equivalent circuit representation of proposed inter-operable multi-utility fast charger in Vehicle-to-Vehicle mode.

Hence, all modes of operation can be achieved without any additional semiconductor switch, passive element or any complex control. Further, it may be observed from Fig. 4.3-4.5 that during high-power fast charging mode, the major power flows through by-pass path and the converter can be designed according to low-power consumption modes. This advantage permits the selection of low voltage and current rated components enabling cost cutting, stress minimization, heat sink size reduction and overall efficiency improvement.

4.2.3 Switching Strategy and Operating Principle of the Proposed Converter

The proposed converter utilizes same switches and passive components for different modes. The PWM strategy of the converter switches in each mode is similar except the switching frequency and the phase shift (leading or lagging). Therefore, the switching of

converter in fast charging mode is explained in detail and that in other two modes are discussed briefly. The key waveforms in each mode are shown in Fig. 4.6.

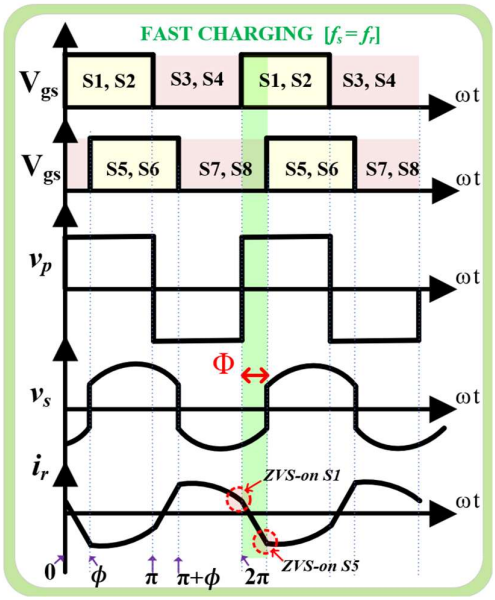

Fig. 4.6 Key waveform of the proposed converter in FPP charging mode.

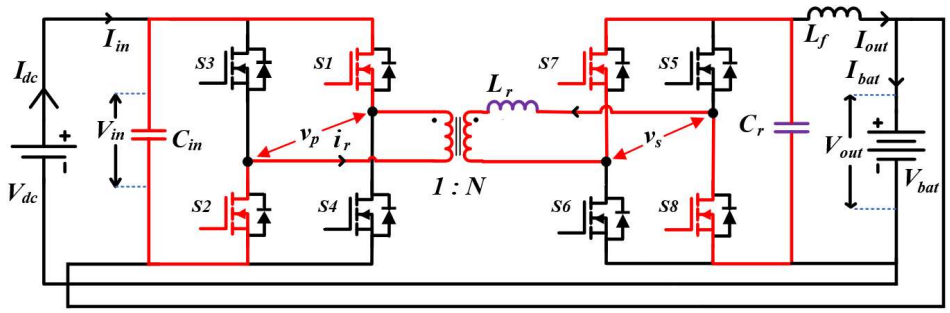

Fig. 4.7 Equivalent circuit of proposed converter in battery charging mode corresponding to operation in fast charging mode in interval I: $0 < \omega t \leq \phi$.

The operation of the converter in FPP based configuration to implement fast charging in one complete cycle can be divided into four intervals, based on the switching instant of primary and secondary bridge switches. The circuit in interval I with active devices are shown in Fig. 4.7. Fig. 4.8 shows the different stages of switching transition to achieve ZVS turn-on. The current flowing through the inductor i_r depends on the differential resonant voltage given by

$$v_{Lr} = v_s - v'_p \tag{4.1}$$

Interval I [$0 < \omega t \leq \phi$]: Initially, switches S7, S8 are assumed to be conducting. Before the beginning of the Interval I at $\omega t = 0$, the inductor current is positive as shown in Fig. 4.6 (a).

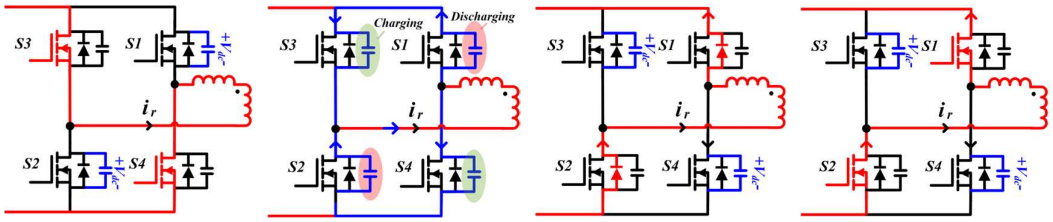

Fig. 4.8 Switching transition demonstrating achievement of ZVS-turn on.

Thus, i_r continues to flow through S3 and S4 and the output capacitance of S1 S2 is completely charged to source voltage V_{dc}, as in Fig. 4.8 (a). As soon as the gate signal of S3 and S4 is turned off, the current stops flowing through its channel. However, the positive flow of inductor current help to charge and discharge the output capacitor of S3-S4 and S1-S2, respectively as in Fig. 4.8 (b). Once the capacitor of S1 S2 is fully discharged, its body diode starts conducting until the deadband period finishes (Fig. 4.8 (c)). At this point the gate signal of S1-S2 reaches threshold voltage and the inductor current flows through its conduction channel, Fig. 4.8 (d). The conduction of diode before switch turn-on results in zero voltage across the switch, enabling ZVS turn on of S1 and S2. As switches S1 and S2 are conducting, the primary voltage is given by $v_p = V_{in}$, as in Fig. 4.7. This causes the inductor current to decrease with a steep slope governed by resonant inductor voltage $v_{Lr} = -v_s - v'_p$, causing the. The current continues to decrease and crosses zero to charge the inductor with opposite polarity. This mode ends until $\omega t = \phi$ when the switches S7 S8 are turned off.

Interval II [$\phi < \omega t \leq \pi$]: The circuit with its active switches in this interval is shown in Fig. 4.9. As soon as S7 S8 is turned off at $\omega t = \phi$, the lagging current discharges the output capacitor of S5 S6 and eventually flows through the body diode of S5 S6. Switches S5 S6 are gated at ϕ, and the current flows through the channel of the MOSFET. As the inductor current is negative at $\omega t = \phi$, conduction of body diode of S5 and S6 is ensured, thereby confirming ZVS-turn on of secondary switch. S5 S6 conduction causes the resonant inductor voltage to become $v_{Lr} = v_s - v'_p$, resulting in inductor current to rise

with a positive slope. This interval continues till $\omega t = \pi$, when S1 S2 are turned off, and S3 S4 are tuned on.

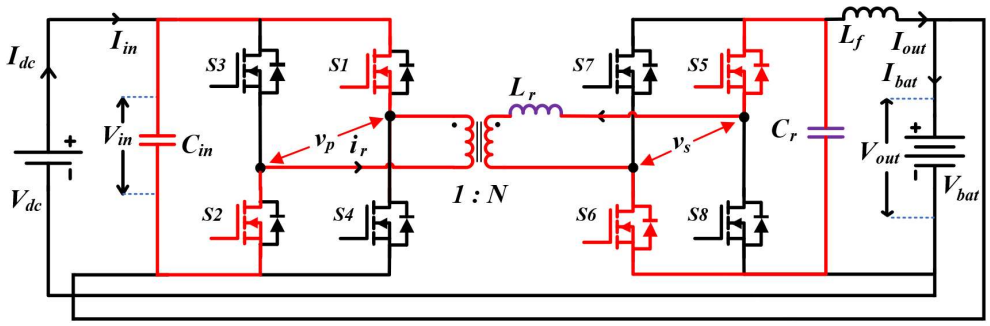

Fig. 4.9 Equivalent circuit of proposed converter in battery charging mode corresponding to operation in fast charging mode in Interval II.

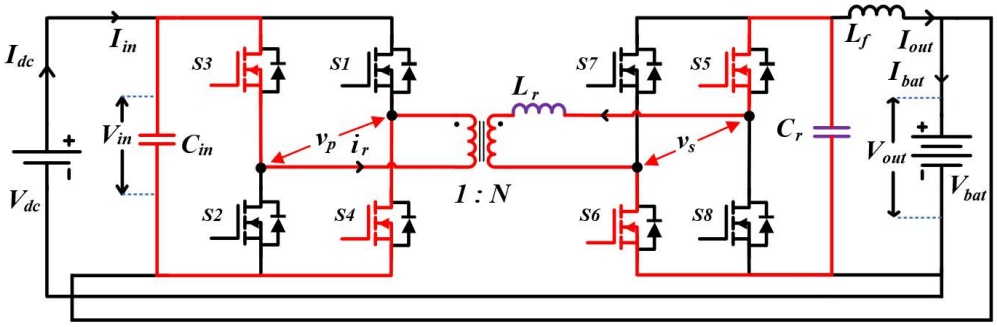

(a) Interval III: $\pi < \omega t < \pi + \phi$.

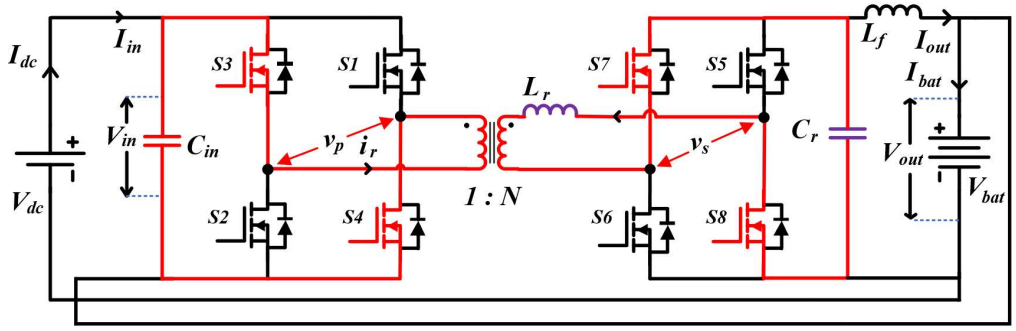

(b) Interval IV: $\pi + \phi < \omega t \leq 2\pi$.

Fig. 4.10 Equivalent circuit of proposed converter in battery charging mode corresponding to operation in fast charging mode in (a) & (b) Interval I (c) Interval II.

Due to the symmetrical configuration of the proposed converter, the operation of the converter is similar in other half cycle of the transformer voltage, i.e., in interval III and

interval IV, respectively, until $\omega t = 2\pi$. The circuit corresponding to the other half of the switching cycle in each interval is shown in Fig. 4.10 (a) and (b).

In V2Aux mode, as in Fig. 4.11, the switching frequency is half of the resonant frequency and the secondary bridge is voltage v_s is leading with respect to v_p. Further, the inductor current is negative at $\omega t = 0$, showing S5 S6, turning on at zero voltage. In addition, at the $\omega t = \pi + \phi$, when the switch S1 S2 are turned-off, again the current crosses zero, thus ensuring ZCS turn-off. Hence, this mode of operation has higher converter efficiency due to elimination of both turn-on and turn-off losses.

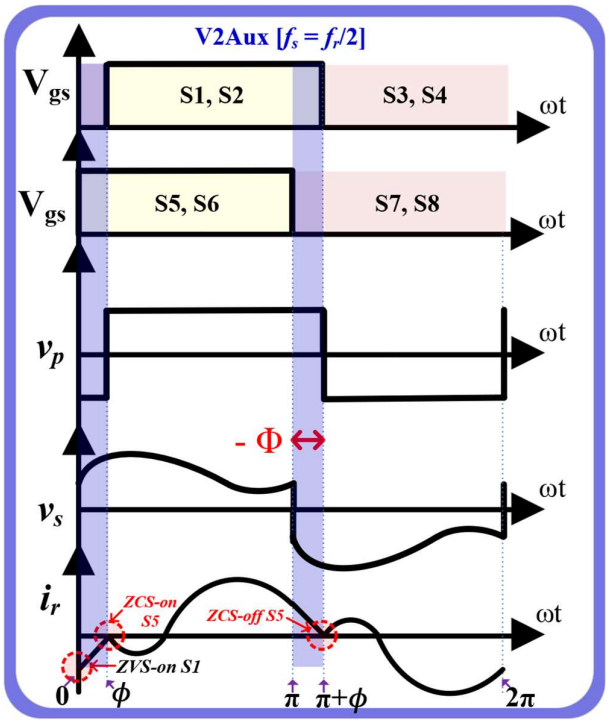

Fig. 4.11 Key waveform of the proposed converter V2Aux mode.

Further, ***in V2V mode***, the converter again switched at resonant frequency, however, at leading phase shift to ensure CC operation in reverse power flow mode, as show in Fig. 4.12. At $\omega t = 0$, when the converter is turned on, current i_r is negative indicating conduction of diode of S5 S6, thus ensuring ZVS turn on of S5 S6. Similarly, other all other switches achieve ZVS turn-on in V2V mode.

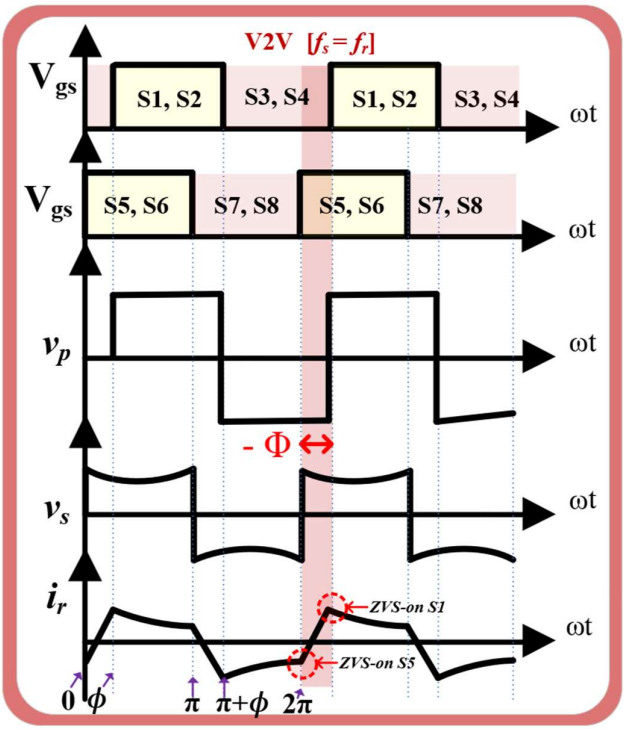

Fig. 4.12 Key waveform of the proposed converter V2V mode.

4.3 Performance Analysis of the Proposed Charger

4.3.1 Performance as a Current Source and a Voltage Source

The behavior of converter as a current source in fast charging and V2V mode and voltage source in V2Aux mode is due to the parallel resonance feature of the proposed converter. Fig. 4.13 (a) and (b) represents the equivalent circuit of proposed converter in FPP configuration and full power processing configuration.

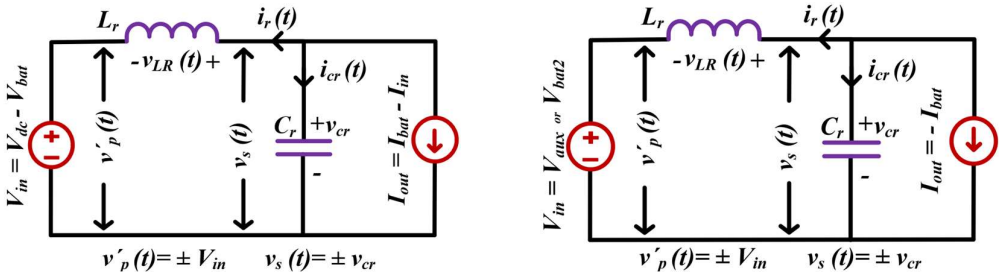

Fig. 4.13 Equivalent circuit of the proposed converter in (a) fast charging mode (b) V2Aux and V2V mode.

The circuit behavior can be established using the following equation

$$L_r \frac{di_r(t)}{dt} = v_s(t) - v'_p(t) \tag{4.2}$$

$$C_r \frac{dv_{cr}(t)}{dt} = i_r(t) - I_{out} \tag{4.3}$$

Where, i_r and v_{cr} represents the resonant current and voltage. The characteristics impedance of the tank circuit is $Z_o = \sqrt{L_r/C_r}$ and resonant frequency of the tank is given by $\omega_o = 1/\sqrt{L_r C_r}$.

Upon deriving (4.2) and (4.3) for each switching states and solving the subsequent differential equations, we obtain normalized load voltage (M) and normalized load current (J) equations given as

Normalized Current (J):

$$J = \frac{I_{out}\, Z_o}{V'_{in}} \tag{4.4}$$

Also,
$$\phi = sin^{-1}\left(cos\frac{\gamma}{2} + J\ sin\frac{\gamma}{2}\right) \tag{4.5}$$

Normalized Voltage (M):

$$M = \frac{V_{out}}{V'_{in}} = \frac{2}{\gamma}\left(\left(\frac{\pi}{2} - \phi\right) - \frac{\cos\phi}{\cos\frac{\gamma}{2}}\right) \tag{4.6}$$

$$\gamma = \frac{\pi}{f_s/f_r} \tag{4.7}$$

The above equations are utilized to plot the output characteristics of the converter for varying normalized output current and voltage as shown in Fig. 4.14.

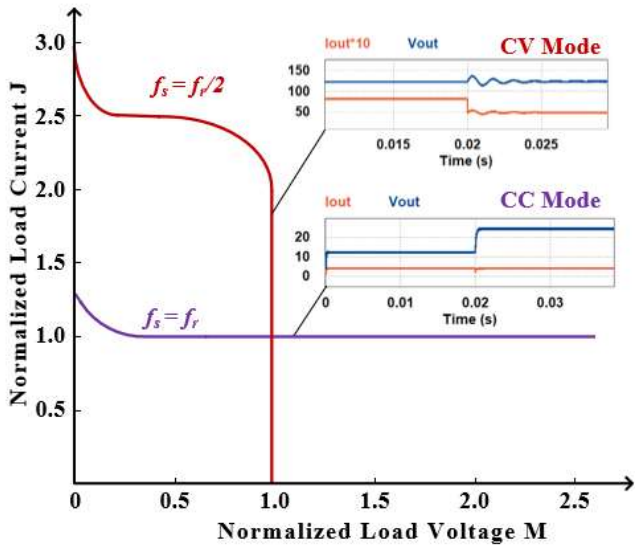

Fig. 4.14 Behavior of converter as current source and voltage source.

It may be observed that at resonant frequency the characteristic is parallel to M (voltage) axis, which means the current remains constant as the voltage varies, i.e., CC output from the converter. Further, for half-resonant frequency, the M-J characteristics becomes parallel to J axis, indicating constant voltage operation with varying current, thus validating the constant voltage behavior of the converter.

The output of the converter at resonant frequency is given by

$$J = \sin\phi \tag{4.8}$$

i.e.,

$$I_{out} = \frac{n\,V_{in}}{Z_o}\sin\phi \tag{4.9}$$

Similarly, in the CV mode of operation, the normalized voltage gain of the converter becomes constant and is given by

$$M = \frac{V_{out}}{V'_{in}} = 1 \tag{4.10}$$

or

$$V_{out} = N\,V_{in} \tag{4.11}$$

These equations verify the behavior observed in the load characteristics. Hence, this dual source property of the parallel resonant tank is utilized to implement different operating modes as discussed in section 4.2.2.

4.3.2 Performance as a Fractional Power Processor

The performance analysis and comprehensive comparison of the proposed charger with conventional approach gives an optimal design solution for a multi-utility charger. The parameters relating to the proposed FPP configuration are calculated by invoking KCL and power balance at the input-output node of the FPP-configured converter. The obtained results are compared with conventional full power processing converter and is presented in Table 4.1. Further, the performance analysis of proposed configuration is presented by considering a charging scenario of 50 kW, 400 V battery that utilizes the

Table 4.1 Comparison: FPP Mode Converter vs Full Power Processing Converter

	Conventional Converter	FPP Converter
$\boldsymbol{I_{out}}$	I_{bat}	$\frac{\eta\,(V_{dc}-V_{bat})\,I_{bat}}{(1-\eta)\,V_{bat}+\eta\,V_{dc}}$
$\boldsymbol{I_{in}}$	$\frac{V_{bat}I_{bat}}{\eta V_{dc}}$	$\frac{V_{bat}\,I_{bat}}{(1-\eta)\,V_{bat}+\eta\,V_{dc}}$
Fractionality Ratio $\boldsymbol{K = P_{in}/P_{bat}}$	1	$\frac{(V_{dc}-V_{bat})}{(1-\eta)\,V_{bat}+\eta\,V_{dc}}$
System Efficiency η_{sys}	η	$\frac{(\eta-1)V_{bat}+V_{dc}}{\eta\,V_{dc}}$

converter operating with efficiency of 95 %.

4.3.3 Behavior with Varying Fractionality Ratio, K

A critical parameter associated with the performance of FPP configured converter is the fractionality ratio, K, which is defined as the ratio of power handled by the converter (P_{in}) to the total power delivered to the battery in fast charging mode. It determines the

overall system efficiency, i.e., lower is the K value, less is the power processed, thus, less losses and higher efficiency.

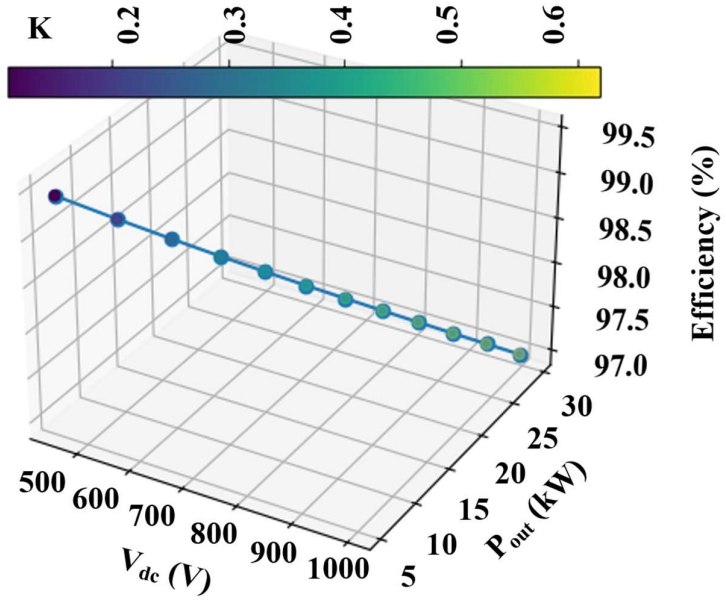

Fig. 4.15 Performance analysis of proposed charger in FPP mode for 50 kW FC.

Fig. 4.15 presents the variation of K with source voltage (V_{dc}) and its effect on the system efficiency, for a 50 kW of power delivered to 400 V battery. It may be observed that, for $K = 0.11$, 450 V input, and 5.3 kW P_{out} the proposed configuration provides a significant increment in efficiency of 4.4%, leading to 99.4 %. Another notable point is the adaptability of proposed FFP based configuration for the fast-charging application of 50 kW, with converter ranging from slow OBC of 7.2 kW ($K = 0.15$) to Level II OBC charger of 22 kW ($K = 0.44$).

Further, the relationship between the fractionality ratio i.e., the amount of power processed by the converter and the input voltage can be established as

$$K = \frac{(V_{dc} - V_{bat})}{(1-\eta)\, V_{bat} + \eta\, V_{dc}} < 1 \tag{4.12}$$

$$(V_{dc} - V_{bat}) < [(1-\eta)\, V_{bat} + \eta\, V_{dc}] \tag{4.13}$$

$$(V_{dc} - V_{bat}) < (2-n)\, V_{bat} \tag{4.14}$$

$$V_{dc} < \left[1 + \frac{1}{(1-\eta)}\right] V_{bat} \tag{4.15}$$

From the above relation it may be concluded that the proposed topology can achieve fractional power processing behavior for wide range of source voltage. In other terms, fractional power processing behavior can be achieved for wide range of battery voltage for a given dc source voltage.

4.4 Design of the Proposed Charger

The voltage and current stress across switching devices are the major cause of losses, and weight owing to thermal dissipation and heat sink requirement. In addition, the component cost increases sharply with the increase in voltage and current ratings. Further, as MOSFET voltage rating increases, its $R_{ds\text{-}on}$ increases significantly leading to higher conduction losses. Increase in current stress further results in high I^2R losses. One of the main advantages offered by the proposed charger is the reduction in current and voltage stress of the charger while handling large power required for FC. To extensively benefit from the FPP approach in optimally designing the proposed inter-operable multi-utility charger, it is critical to consider the ratings of operation in all three modes and select optimal design parameter, that would result in cost cutting and compact design, while ensuring safe and efficient operation.

4.4.1 Selection of the Switches

To enable high frequency operation with lower power handling, MOSFETs are the optimal choice of switching device. Further, to avoid over-rated component selection while incorporating all modes the voltage across and current through the converter in each mode is calculated and is given in Table 4.2. For present scenario, a case is considered when similar EV (to source) is being charged in V2V mode. Here selection of input bridge switches is made based on following conditions,

$$V_{in-max} = \begin{cases} V_{dc} - V_{bat}, & V_{dc} > 2\,V_{bat} \\ V_{bat}, & V_{dc} < 2\,V_{bat} \end{cases} \tag{4.16}$$

Depending on the above conditions, the switch voltage rating can be selected. Here, a significant reduction in input voltage is obtained from V_{dc} in conventional full power processing converter case to $V_{dc} - V_{bat}$ or V_{bat} in proposed converter. Further, maximum switch current flows through the converter input during CC operation in fast charging mode, as $I_{in} = I_{dc}$. However, the current I_{in} in FPP fast charging mode is further dependent on fractionality ratio K, and input voltage as also reflected in Fig. 4.16.

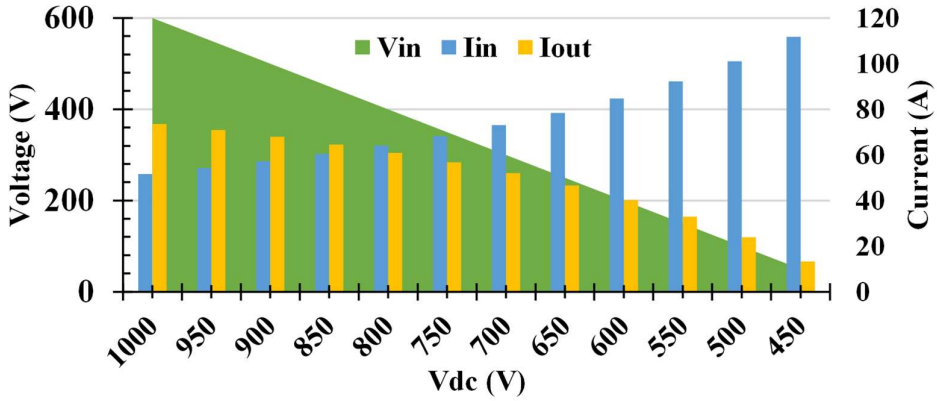

Fig. 4.16 Voltage and current analysis for component selection of the proposed converter based on performance in FPP mode.

Table 4.2 Converter Metrices in Each Mode

	Primary Bridge		Secondary Bridge	
	$\boldsymbol{V_{in}}$	$\boldsymbol{I_{in}}$	$\boldsymbol{V_{out}}$	$\boldsymbol{I_{out}}$
Conventional OBC $\boldsymbol{V_{dc} < V_{bat}}$	V_{dc}	I_{dc}	V_{bat}	I_{bat}
FPP Fast Charging $\boldsymbol{V_{dc} > V_{bat}}$	$V_{dc} - V_{bat}$	I_{dc}	V_{bat}	$I_{bat} - I_{dc}$
Vehicle to Auxiliary $\boldsymbol{V_{aux} < V_{bat}}$	V_{aux}	$-I_{aux}$	V_{bat}	$-I_{bat}$
Vehicle to Vehicle $\boldsymbol{V_{bat2} < V_{bat}}$	V_{bat2}	$-I_{bat2}$	V_{bat}	$-I_{bat}$

The secondary bridge in all three mode is subjected to battery voltage V_{bat}, however, only differential current flows through it in high power fast charging mode, thereby

resulting in significant reduction in switch current rating, as can be observed in Fig. 4.16, where output current is 13 A for $V_{dc} = 450\,V$, $K = 0.11$ as opposed to 110 A for conventional full power processing converter (450 V, 50 kW).

4.4.2 Choice of Transformer Turn Ratio

The output of the converter in full power processing constant voltage mode is governed by the turn ratio as in (4.17). Therefore, transformer turn ratio is calculated based on terminal voltage in this mode as

$$N = \frac{V_{out}}{V_{in}} = \frac{V_{bat}}{V_{aux}} \tag{4.17}$$

For the laboratory developed prototype, the proposed concept is verified considering 72 V nominal voltage battery, with vehicle auxiliary voltage of 48 V. Therefore, the transformer ratio is selected as 1.6.

4.4.3 Choice of Resonant Tank Parameters

The tank parameters depend on the operation frequency and power rating. Higher the switching frequency smaller is the size of magnetic component. The resonant inductor current is inversely proportional to the tank characteristic impedance Z_o. In the present application, the V2Aux mode of operation is a low power application, however, the V2V mode and fast charging mode operate at higher power, and constant current for a given ϕ. Considering a design point where converter operates at low K value in fast charging mode, the highest current flows through the converter in V2V mode. Therefore, considering a case with two vehicles having same battery nominal voltage, 72 V

$$Z_o = \frac{N\,V_{out} * \sin\phi}{I_{in}} = \frac{N\,V_{bat} * \sin\phi}{I_{V2V}} \tag{4.18}$$

Where, V_{bat} is the source battery voltage, ϕ is the phase shift and I_{V2V} is the current supplied to discharged battery. Further, if the power handled by converter is higher in fast charging mode compared to V2V mode, Z_o is calculated as

$$Z_o = \frac{N\,V_{out} * \sin\phi}{I_{in}} = \frac{N\,V_{bat} * \sin\phi}{I_{dc}} \tag{4.19}$$

Based on the calculated Z_o value, the tank parameters can be calculated using $Z_o = \sqrt{L_r/C_r}$ and $\omega_o = 1/\sqrt{L_r C_r}$, the required leakage inductance L_r and resonant capacitance C_r can be found to transfer the desired power.

4.4.4 Impact of Integration on Converter Performance and Lifetime

In actual application OBCs are active only for about 10-20% of their designed operational life and therefore can easily outlast the service life of EV with significant underutilization. The proposed integration of multiple functions, especially the low power and less frequent functions such as V2Aux, V2V and even FPP based fast, into a single converter reduces the cost and volume of the on-board power electronics and at the same time equip EV with all the functions that may not be frequently required but greatly alleviate the overall EV driving experience. As the converter operates independently in each mode and well below the OBC rating, it can operate for OBC lifetime reliably and heat generation can be effectively managed. Any potential limitation of integration can be further addressed with slight component de-rating, multi-layer track design and thermal via for further efficient design and performance.

4.5 Experimental Validation

Based on the above design criteria, a scaled-down laboratory prototype of proposed multi-utility charger is developed and shown in Fig. 4.17, with design parameters as given in Table 4.3. A 72 V battery is emulated using ITECH IT6006C battery emulator to validate the behavior of the proposed charger in all three operating modes matching the commercially available battery standards. Microprocessor TMS320F28335 is employed to generate the PWM signals for switching MOSFETs.

4.5.1 Performance Validation of FPP Fast Charging Mode

4.5.1.1 Steady State Performance Validation in FC mode

Fig. 4.18 shows the steady state results when the 72 V battery is charged at 650 W with a source voltage of $V_{dc} = 120\,V$. The parameters are as shown in Fig. 3. The peak

primary and secondary voltage, v_p and v_s reflect the voltage stress on the switches S1-S4 and S5-S8, respectively.

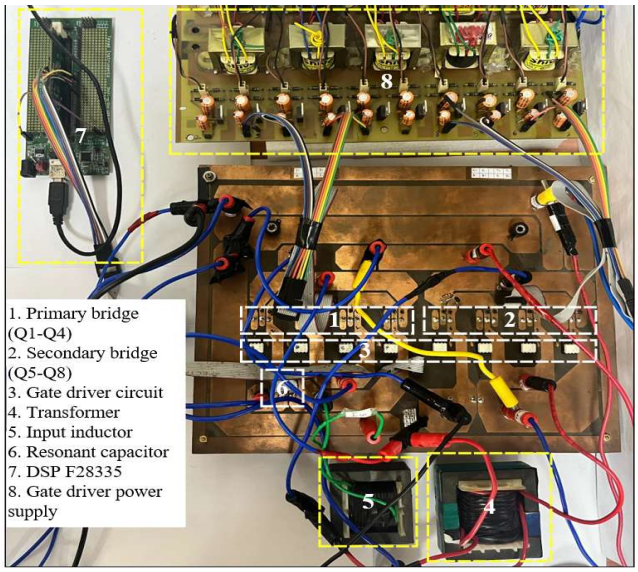

Fig. 4.17 Photograph of the laboratory developed prototype of proposed inter-operable multi-utility charger.

Table 4.3 Charger Design Parameters

Component	Value	Component	Value
Inductor, L_f	1.3 mH	Battery Voltage, V_{bat}	72 V
Capacitor, C_{in}	94 µF	Source Voltage, V_{dc}	120 V
Turn ratio, N	16:10	Auxiliary Voltage, V_{aux}	48 V
Resonant Frequency, f_r	89 kHz	Switching Frequency	
Characteristic Impedance, Z_o	8.89 Ω	f_s (fast charging)	89 kHz
Leakage Inductance, L_r	16 µH	f_s (V2Aux)	44.5 kHz
Resonant Capacitor, C_r	202 nF	f_s (V2Aux)	89 kHz

The converter operates at resonant frequency $f_s = 89\ kHz$ and secondary bridge lags the primary by phase shift of 30°. The RMS value of secondary resonant voltage is equal to the battery voltage. It may be observed that the primary bridge is subjected to difference

voltage resulting in the voltage stress across switch S1 to be 48 V, whereas the secondary switch voltage stress is 79 V. It may be concluded from the result that despite the source voltage is 120 V the input bridge voltage is reduced to 48 V resulting in significant reduction in stress, verifying the proposed concept. i_{rs-pe} represents the current stress on the secondary switches. It may further be observed that when the switch S1 is turned on at $\omega t = 0$, the inductor current is positive reflecting the anti-parallel diode, thus confirming ZVS turn-on as discussed in section II.C. Further, when S5 is turned on at $\omega t = 0$, the current is negative, thus flowing through anti-parallel diode of S5 ensuring ZVS turn on. The converter achieves a significantly higher efficiency of 98.87 % in FC mode.

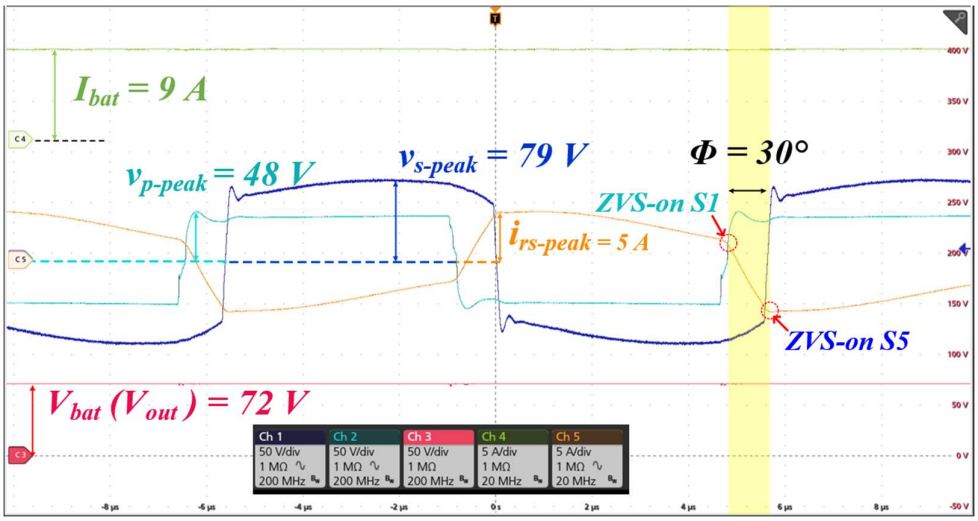

Fig. 4.18 Experimental results verifying steady state operation of proposed multi-utility charger in fast charging mode, for $V_{bat} = 72\ V, 650\ W$.

4.5.1.2 Dynamic Performance Validation in FC mode

In Fast charging mode, multi-step CC charging is a popular strategy to ensure fast and optimal charging, where in the battery is charged at high valued constant current and as the SOC increases the current is decreased in steps to prevent large heat generation due to increasing high internal resistance during charging. Fig. 4.19 shows the stable operation of the converter in the presence of dynamics, i.e., by varying phase shift during charging to achieve battery current regulation. It may be observed that the current decreases from 12.5 A to 9.5 A as the phase shift is decreased from 45° to 30°, thus, confirming CC behavior of the converter.

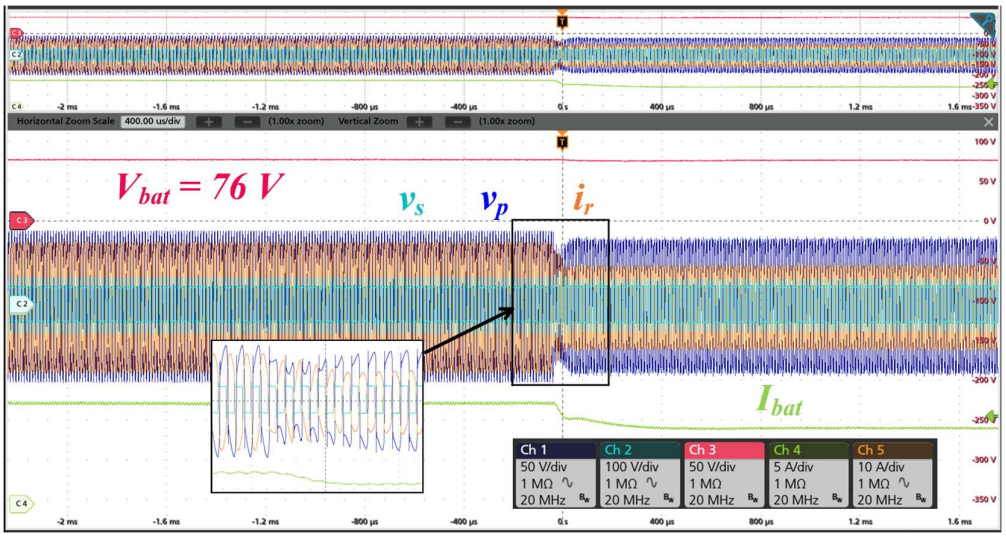

Fig. 4.19 Performance of converter for dynamics at $\phi = 45°$ to 30°.

4.5.1.3 Operation at Varying Fractionality (K)

The charger performance in FC mode is characterized by fractionality ratio or the amount of power processed through the converter with respect to total delivered power to battery. Fig. 4.20 (a) and (b) demonstrate the operation at $K = 0.25$ and $K = 0.48$, when charging a battery of nominal voltage of 48 V with $V_{dc} = 70\,V$ and $V_{dc} = 100\,V$, respectively. It may be observed that for wide range of K both the bridges achieve ZVS thereby maintaining high efficiency charging.

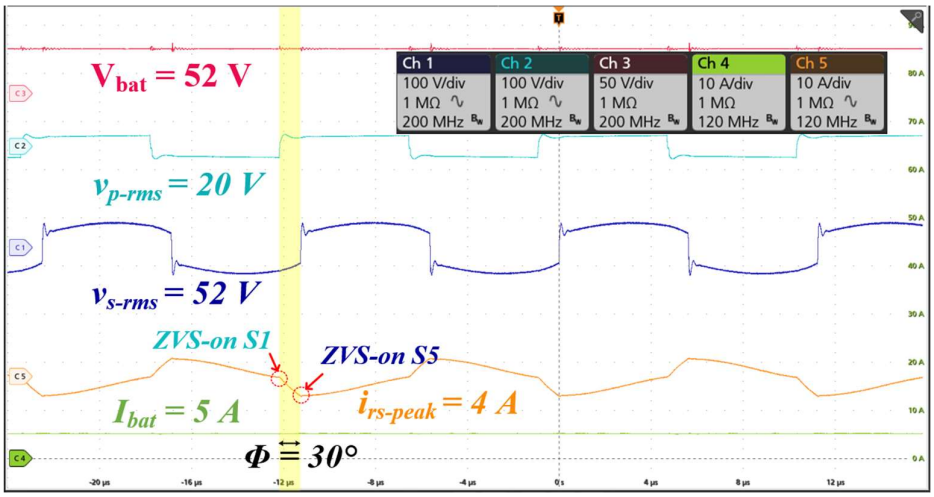

(a)

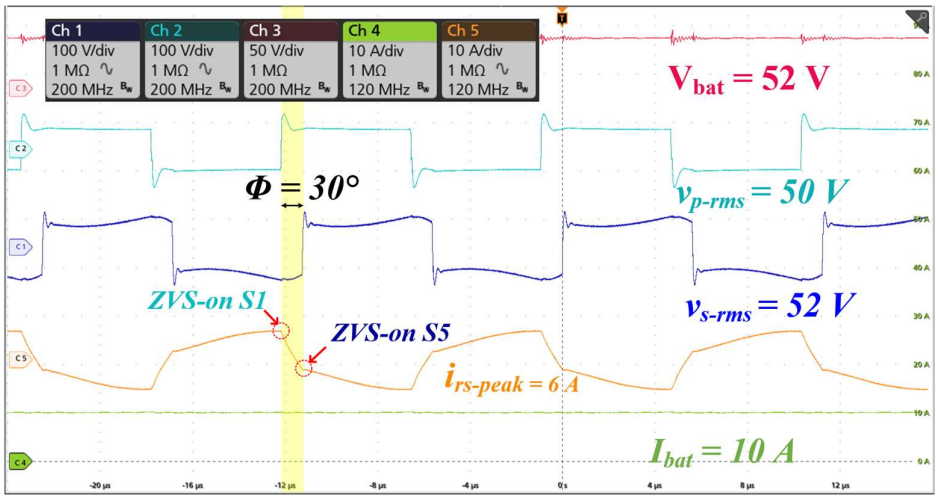

(b)

Fig. 4.20 (a) Operation in FC mode for fractionality ratio K = 0.25, $V_{bat} = 52\ V$*. (b) K = 0.48,* $V_{bat} = 52\ V$*.*

4.5.2 Performance Validation of Charger in V2Aux mode

4.5.2.1 Steady State Performance Validation in V2Aux mode

(a) Steady State Performance Validation in V2Aux mode

Fig. 4.21 shows the steady state result when charged battery with terminal voltage 80 V is feeding a resistive load at 48 V with 4.8 A current, thus, charging at 230 W. The converter is operating at half resonant frequency, i.e., 44.5 kHz, with primary bridge leading the secondary with $\phi = -5°$, resulting in reverse power flow, feeding the load at constant voltage. As the converter works in reverse power flow, the load voltage of 48 V appears at the input V_{in}. The RMS primary and secondary voltages are 48 V and 78 V, respectively. The stress on primary and secondary switches are 52 V and 104 V, respectively. The peak current through secondary bridge is 5.9 A. Further, it may be observed that when S5, S6 is turned on at $\omega t = -5°$, the current is negative, indicating diode conduction and therefore, ZVS operation of secondary bridge switches. Further, at $\omega t = 0$, when switch S1, S2 are turned on the current reaches zero, confirming ZCS turn-on of primary switches. In addition, at $\omega t = \pi$, when S1 S2 is turned off, again the current reaches zero ensuring ZCS turn-off of primary switches. The converter achieves a significantly higher efficiency of 98.12 % in V2Aux mode as turn-off losses are also eliminated.

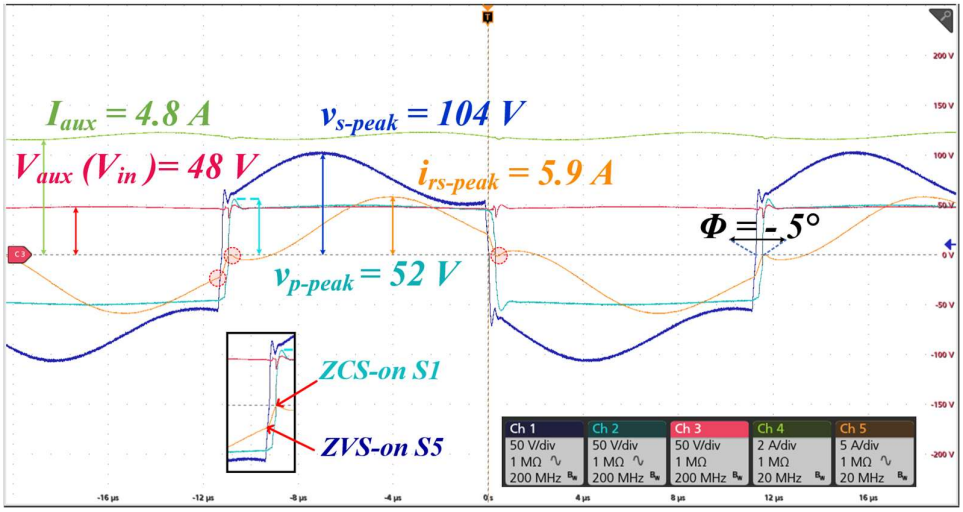

Fig. 4.21 Steady state results verifying operation of proposed multi-utility charger in V2Aux mode for V_{bat} = 72 V V_{aux} = 48 V, at 230 W.

4.5.2.2 Dynamic Performance Validation in V2Aux mode

The various auxiliaries are turned on and off at different instants depending on the requirement. During this operation the terminal voltage should remain constant irrespective of the change in load. To verify the stable performance of the converter during load variation, converters' dynamic results are presented in Fig. 4.22. It may be observed that the load voltage remains stable at 48 V while the current changes for 25 % change in load demand demonstrating superior performance.

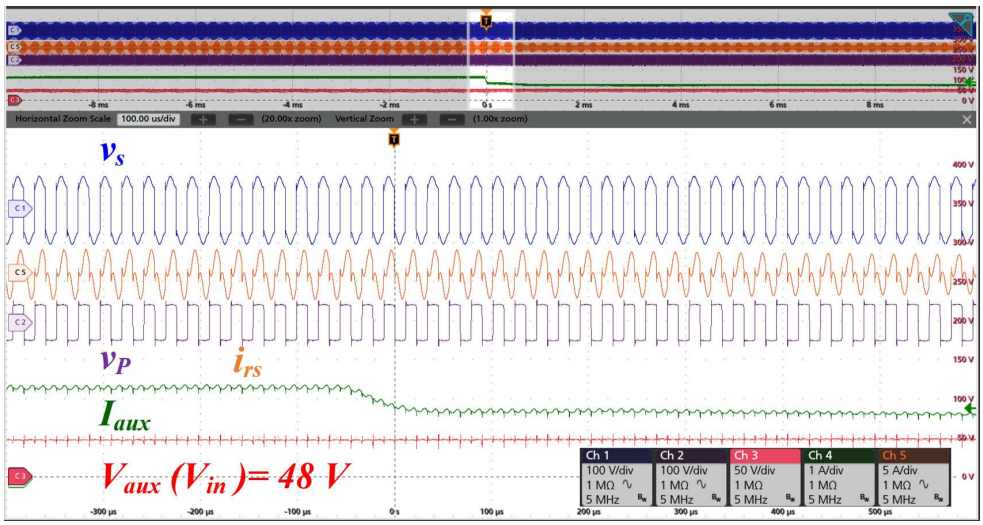

Fig. 4.22 Converter dynamic performance in CV mode with f_s = 44.5 kHz when auxiliary load demand changes for 25 % of load current.

4.5.3 Performance Validation of Charger in V2V mode

4.5.3.1 Steady State Performance Validation in V2V mode

Fig. 4.23 shows the converter behavior in V2V mode, when a discharged battery of 72 V nominal voltage is charged with 72 V source battery. The converter operates at resonant frequency, and $\phi = -45°$, to ensure reverse flow and constant current operation, as is required to add quick charge to a battery in emergency situation. In V2V mode, the RMS primary voltage is observed as 70 V and the RMS secondary voltage is 79.8 V. The primary switch stress is observed to be 120 V and secondary switch stress is 125 V. The peak current stress is 13.76 A in secondary switch to deliver 350 W to the load battery. In addition, the inductor current is negative at $\omega t = -45°$, when switch S5, S6 is turned on, indicating ZVS turn on of the primary bridge switches. Similarly, at $\omega t = 0$, when S1 S2 is turned on the current is positive indicating ZVS turn on of primary bridge switches.

Further, Fig. 4.24 shows the adaptability of V2V operation to support other batteries at lower voltage, when a 48 V battery is being charged in CC mode, with $\phi = -45°$, at $I_{bat2} = 4.8\,A$. It may be observed the converter works satisfactorily, and both primary and secondary bridge switches achieve ZVS for this operating case also. Converter achieves an efficiency of 97.2 % in V2V mode.

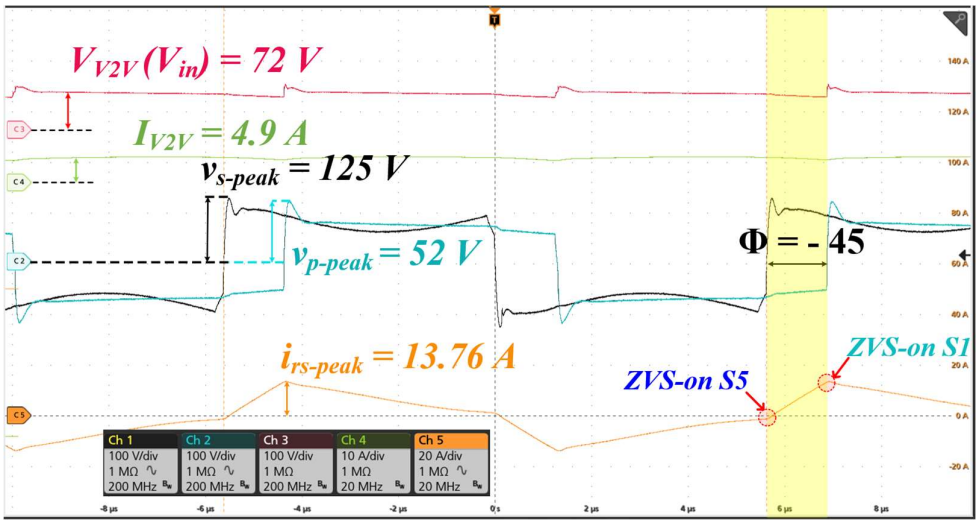

Fig. 4.23 Experimental results verifying steady state operation of proposed multi-utility charger in V2V mode with $V_{bat} = 72\ V$ $V_{V2V} = 72\ V, 350\ W$.

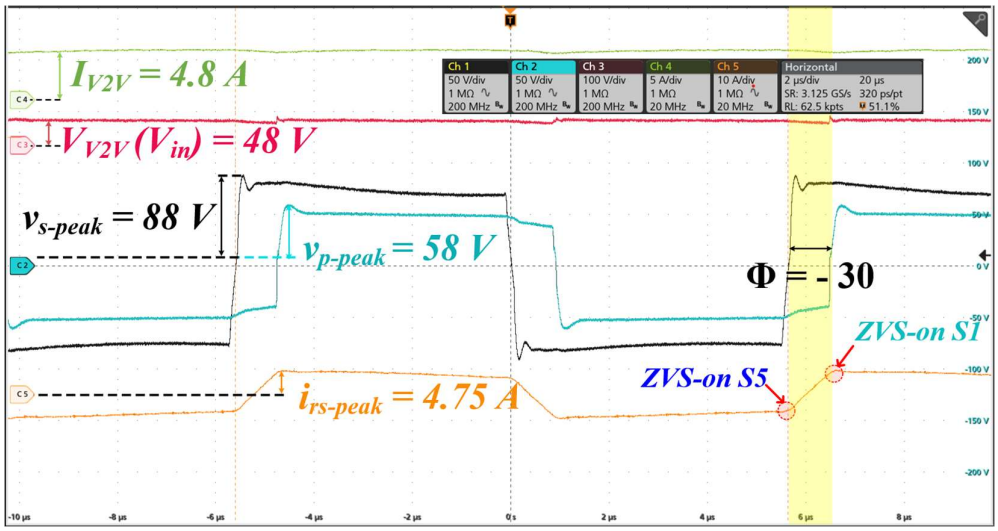

Fig. 4.24 Experimental results verifying steady state operation of proposed multi-utility charger in V2V mode with $V_{bat} = 72\ V$, $V_{V2V} = 48\ V, 230$.

4.5.3.2 Dynamic Performance Validation in V2V mode

To verify the constant current behavior in V2V mode, with load battery of 48 V, the load battery current is controlled by varying phase shift from 20° to 45°, as shown in Fig. 4.25. The current changes from 3.8 A to 7 A while maintaining stable converter current and voltage thus, demonstrating robust charger performance in V2V CC mode.

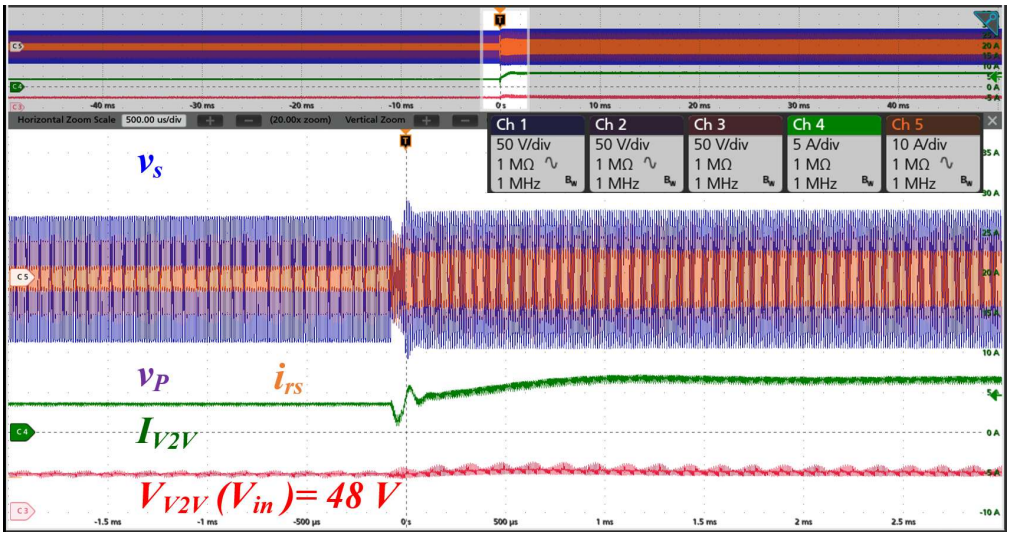

Fig. 4.25 Dynamic performance of converter for V2V CC mode, $f_s = 89\ kHz$ *for phase shift variation from* $\phi = 20°$ *to 45°.*

Table 4.4 Comparison Among the Proposed Topology and Other Chargers

		Ref.	Modes			Switch Count	Passive Comp.	Efficiency (%)			Control
			EV Charging	V2Aux	V2V			EV Charging	V2Aux	V2V	
Full Power Processing	I	[104]	G2V (DC/DC only)	✓	X	12	7 C	96 %	93.3 %	X	Complex (5) x (PI)
		[22]	G2V (AC/DC+DC/DC)	✓	X	4 + 4*	3 C + 3 L	95 %	65-82 %	X	Complex (2) x (PI)
		[135]	Slow (AC/DC+DC/DC)	✓	✓	12 + 2*	4 C + 4 L	97.2 %	97 %	96.1 %	Complex
	II	[92]	On-board Fast Charging (AC/DC+ DC/DC)	X	X	3 + 5 Diode	3 C + 4 L	93.5 %	X	X	PI controller
		[136]	Combined AC and DC Fast Charging	X	X	8 + 6*	2 C + 4 L	95.79 %	X	X	(4) x Compensator
Fractional Power Processing	III	[137]	OBC DC Charging	X	X	8	2 C +1 L	99 %	X	X	PI Controller
		[138]	OBC DC Charging	X	X	8	2 C + 1 L	96 %	X	X	-
	IV	[139]	Fast Charging	X	X	4 + 2*	3 C + 1 L	99.2 %	X	X	LUT** + PI
	V	Prop.	OBC Fast Charging	✓	✓	8	2 C + 2 L	98.87 %	98.12 %	97.2 %	Simple

* Indicates additional switches in ac/dc PFC stage. Prop. = Proposed Charger **LUT= Look up table

I	On-board slow	II	On-board fast	III	On-board slow	IV	Off-board fast	V	On-board fast

4.5.1 Comparison and Discussion

Table 4.4 compares the literature on existing on-board fast chargers and multi-utility chargers that perform V2aux and V2V charging. It may be observed that there is a gap of power processor that can perform both slow and fast charging as well as support V2Aux and V2V capability. Further the improvement of efficiency due to fractional power processing is commendable. When compared in terms of controller complexity, the proposed charger offers a simple solution due to its inherent dual source property of CC and CV behavior.

4.6 Conclusion

This chapter presents an inter-operable multi-utility fast charger based on resonant dual active bridge converter that provides the flexibility to charge the vehicle battery from any of the available charging facility, i.e., ac, dc level 2 or fast charging including both low voltage outlet in rural and high voltage interface at highway charging network. The proposed charger performs high efficiency fast charging while utilizing only OBC rated dc/dc converter. Further, it supplies EV auxiliary loads and support quick V2V charging only by performing single step frequency change and phase-shift control. The proposed charger performs all above functions without requiring additional components or over-stressing existing components. Additionally, the multi-stage CC charging strategy and smooth voltage and current regulation is achieved in each mode by utilizing simple control without requiring dedicated complex controller. The converter achieves soft-switching for all the switches in each mode of operation ensuring high efficiency operations and minimizing heat sink requirement.

The proposed inter-operable multi-utility fast charger is an efficient and versatile solution to futuristic EV applications. In view of scalability, the proposed charger can facilitate the automakers in streamlining production by using a single, versatile OBC design across multiple EV models, potentially lowering costs and improving vehicle economics.

The solution presented in this chapter acts as an on-board interface providing flexibility to charge from either ac slow charging outlet or dc high voltage fast charging facility. The proposed charger addresses the challenge of compatibility when the dc voltage available at the input is higher that the battery voltage. Another approach to enable charging of both high voltage and low voltage battery packs with high efficiency as in

fractional power processing converters is to develop an FPP charger that can enable step up as well as step down charging operation. Therefore, to address this research gap, a novel quad-operative fractional power processor is proposed in the next chapter.